Macromolecules

Article

pubs.acs.org/Macromolecules

All Plant Oil Derived Epoxy Thermosets with Excellent Comprehensive Properties

Xin-Yi Jian, Xu-Pei An, Yi-Dong Li, Jia-Hui Chen, Ming Wang, and Jian-Bing Zeng*

School of Chemistry and Chemical Engineering, Southwest University, Chongqing 400715, China

Supporting Information

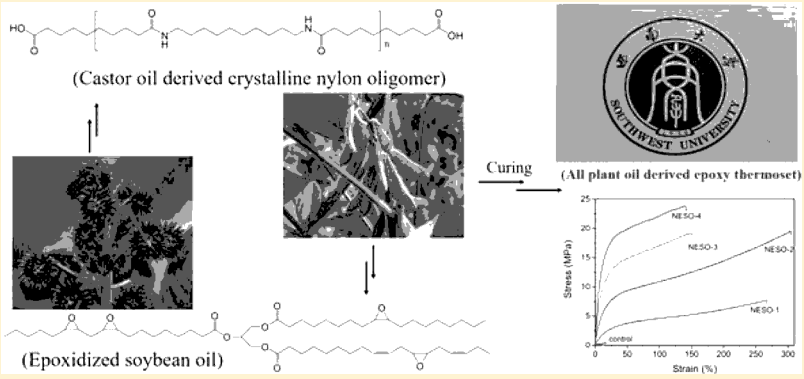

ABSTRACT: Epoxidized plant oil (EPO) thermosets usually exhibit poor performance due to the short, brittle, and amorphous cross-link structures. To fabricate fully biobased high performance EPO thermoset, we synthesized dicarboxyl-terminated polyamide1010 (NYL) oligomers from castor oil derived monomers, i.e., sebacic acid and decamethylene diamine, and used the NYL to cure epoxidized soybean oil (ESO) to fabricate all plant oil derived epoxy thermoset through a catalyst-free curing method. Chemorheological study indicated that the curing rate decreases with increasing NYL chain length. The cross-link density of the epoxy thermoset decreases while the crystallization enhances with increasing NYL chain length, which results in drastic enhancement in tensile strength, Young's modulus, and elongation at break of the resultant thermosets, enabling those parameters to enhance by up to 59, 145, and 18 times, respectively, compared to sebacic acid cured ESO thermoset. The melting temperature and thus the heat resistance of the thermosets are also enhanced obviously with increasing NYL chain length. In addition, the thermosets show good durability and excellent thermal stability. With excellent comprehensive properties, the all plant oil derived epoxy thermosets could find some structural applications other than adhesive and coating.

1. INTRODUCTION

Thermosets with permanent network structure possess superior dimensional stability, mechanical properties, and environmental resistance, which make them irreplaceable in numerous applications, such as aircraft industry, high performance composite, and solar cell encapsulant.[1,2] Epoxy thermosets produced by curing of epoxy resins with suitable curing agents represent an important type of thermoset, which have found a variety of applications, such as coatings, adhesives, electronics, electrical appliances, and high performance composites due to their superior and tunable physical and mechanical properties.[3,4] Therefore, the global production of epoxy thermosets has been increasing quickly and was evaluated to reach 3 million tons by 2017.[5]

It is, however, worth noting that about 90% of epoxy thermosets are produced from nonrenewable diglycidyl ether of bisphenol A (DEGBA) and are nondegradable due to their network structures. Thus, the rapid growth of epoxy thermosets would not only cause large fossil resource consumption but also lead to thermoset waste accumulation. Furthermore, the feedstocks of DGEBA, i.e., bisphenol A (BPA) and epichlorohydrin, can cause some nonignorable negative effects on living organisms.[6−8] Therefore, exploring safe epoxy thermosets from renewable resources has attracted increasing attention in recent years. Various renewable feedstocks, such as epoxidized plant oils, isosorbide, cardanol, lignin derivatives, terpene, and vanillin, have been used to prepare biobased epoxy thermosets.[4,5,9−20]

Epoxidized plant oils (EPO), with more than three epoxy groups per molecule, are a class of commercially available biobased epoxy resins, which can be used as ideal renewable alternatives to fossil based epoxies because EPO could be easily transformed to epoxy thermosets through suitable chemistry techniques, such as cationic polymerization and curing by small compounds with multifunctional groups.[21−23] Especially, fully biobased epoxy thermosets are available by direct cationic polymerization or curing with renewable curing agents, such as sebacic acid and citric acid.[24−26] Unfortunately, EPO-based

Received: May 22, 2017
Revised: July 13, 2017
Published: July 28, 2017

DOI: 10.1021/acs.macromol.7b01068
Macromolecules 2017, 50, 5729−5738

thermosets usually show poor mechanical properties with low mechanical strength and poor toughness, which limits their practical use to nonstructural applications like coatings and adhesives.[1,23,27−31]

The final properties of epoxy thermosets are strongly dependent on their chemical structures, which are determined by the types of epoxy resins and curing agents.[32] The poor mechanical properties of fully biobased EPO thermosets originate from their short, brittle, and amorphous network structures with high cross-link density and highly flexible chains.[33−36] The highly flexible chains result in low glass transition temperature (T_g) and thus low room temperature mechanical strength. Meanwhile, the high cross-link density makes the backbone of the network very brittle. Increasing efforts have been devoted to explore high performance EPO-based thermosets. Most of the studies focused on increasing their T_gs to make them exist in glassy state at service temperature, thus exhibiting high mechanical strength and modulus, due to the frozen chain mobility,[37−40] for example, using fossil-based epoxy resins[35,37] to partially replace EPO or using some fossil-based rigid curing agents[34,36] to cure EPO to enhance T_g. Although the mechanical strength and modulus could be improved, the toughness remained unimproved or even reduced due to the increased chain rigidity of the network. In addition, the sustainability of the thermosets was partially compromised when fossil-based substances were combined and the safety reduced if BPA-based epoxy resins were incorporated.

Since the amorphous network structure combined with high cross-link density accounts for the poor performance of EPO thermosets, if we decrease cross-link density of the thermosets and make them crystalline by incorporation of long-chained crystalline curing agents, high performance EPO thermosets with balanced mechanical strength and toughness could be anticipated. Because mechanical strength would be enhanced by formation of stiff crystalline domains, the toughness would also be improved upon reduced cross-link density. Meanwhile, the heat resistance would be enhanced as well due to the formation of high melting point crystalline domains.

In order not to reduce the renewability of the thermosets, we synthesized crystalline dicarboxyl terminated polyamide1010 (NYL) oligomers from sebacic acid (SA) and decamethylene diamine (DD) and used the crystalline NYL oligomers to cure epoxidized soybean oil (ESO) directly to prepare crystalline ESO thermosets. Both SA and DD can be derived from castor oil.[41,42] Therefore, all plant oil derived epoxy thermosets with high performance could be expected by curing ESO with the crystalline NYL oligomers. We studied the effect of chain length of NYL oligomer on the curing process, cross-link density, crystallization behavior, and thermal and mechanical properties of the fully biobased epoxy thermosets in detail.

2. EXPERIMENTAL SECTION

2.1. Materials. ESO with average number of epoxy group per molecule of 4.1 was purchased from Micxy Chemical Co., Ltd. (Chengdu, China). Sebacic acid (SA, 98.5%) was obtained from the Micxy Chemical Co., Ltd. Decamethylene diamine (DD, 98%) was obtained from HWRK Chemical Inc. (Beijing, China). Trifluoracetic acid (99%) and D-trifluoroacetic acid were obtained from Adamas Reagent Co., Ltd. D-dimethyl sulfoxide and D-chloroform with tetramethylsilane (TMS) internal reference were obtained from the Micxy Chemical Co., Ltd. *N*,*N*-Dimethylformamide (DMF) with AR grade was purchased from Guanghua Sci-Tech Co., Ltd. (Guangdong China). All chemicals were used without further purification.

2.2. Preparation of Dicarboxyl-Terminated Polyamide1010 Oligomers. Dicarboxyl-terminated NYL oligomer with different chain length was synthesized by direct condensation of SA and DD at 210 °C for 5 h under a N_2 atmosphere. The obtained brittle solid oligomer was grounded to powders prior to curing with ESO. The chain length of NYL oligomer was controlled by feed ratio of DD to SA. Four feeding DD to SA molar ratios, i.e., 1:2, 2:3, 3:4, and 4:5, were used to synthesize the oligomers. For brevity, they were abbreviated to NYL-1, NYL-2, NYL-3, and NYL-4, respectively.

2.3. Curing Behavior of ESO with NYL. Both nonisothermal and isothermal curing behavior of ESO with NYL (with acid/epoxy equivalent ratio of 0.7:1.0) were studied by rheological measurement on a TA DHR-1 instrument. For nonisothermal curing, the development of storage modulus and complex viscosity as a function of temperature were recorded from 100 to 350 °C at a heating rate of 3 °C/min under a frequency of 1 Hz and strain of 0.1%. For isothermal curing, the development of storage modulus and complex viscosity as a function of time were recorded at 210 °C under a frequency and strain of 1 Hz and 0.1%, respectively.

2.4. Gel Fraction Measurement. The development of gel fraction with time during isothermal curing at 210 °C was monitored via a soluble method. The curing was performed in a three-necked round-bottomed flask with mechanical stirrer under N_2 atmosphere. The products were taken out of the flask at predetermined time and were subjected to gel fraction measurement. About 1 g (w_1) sample in 20 mL of DMF in a single-necked round-bottomed flask was refluxed at 150 °C for 2 h to dissolve the non-cross-linked part of the product. The hot solvent/sample mixtures were filtered to isolate the insoluble part of the sample, which was vacuum-dried at 80 °C for 48 h and then weighed (w_2). The gel fraction (G_f) was calculated by

$$G_f = \frac{w_2}{w_1} \times 100\% \quad (1)$$

2.5. Preparation of Sample Sheets of NYL Cured ESO Thermosets. Sample sheets of NYL cured ESO thermosets were prepared via a two-step catalyst-free method. The first step involves preparation of homogeneous mixture by precuring of NYL and ESO with acid/epoxy equivalent ratio of 0.7:1.0 in a 210 °C three-necked round-bottomed flask with mechanical stirring under N_2 atmosphere for ∼10 min. In the second step, the precured homogeneous mixture was further cured in a mold (100 × 100 × 0.5 mm^3) between two hot plates of a flat vulcanizing machine at 210 °C under the pressure of 10 MPa for ∼50 min. For property comparison, a control thermoset consisting of ESO and SA was prepared according to the procedures reported in our previous study.[26]

2.6. Fourier Transform Infrared (FT-IR) Spectroscopy. The FT-IR spectra of the samples were recorded on a RF-5301PC spectrophotometer (Shimadzu, Japan) in a wavenumber range of 4000 to 400 cm^{-1}. The resolution and scanning time were 4 cm^{-1} and 32 times, respectively.

2.7. Transparency Test. UV−vis spectra of the samples were recorded on a UV-2550 spectrometer (Shimadzu, Japan) at room temperature from wavelength of 300 to 800 nm with a scanning rate of 60 nm/min to show the light transmittance. The thickness of specimens was ∼0.5 mm. The normalized transmittance was reported by dividing the experimental data with sample thickness.

2.8. Cross-Link Density Measurements. The cross-link density (γ), defined as the number of moles of effective chains per unit volume, was measured via an equilibrium swelling method. The sample with weight of w_0 and dimension of 10 mm × 10 mm × 0.5 mm was immersed in 30 mL of trifluoroacetic acid for 48 h to achieve swelling equilibrium. The weight (w_1) of swollen sample was measured after removal of the surface solvent with filter paper. The swollen sample was then vacuum-dried at 60 °C overnight to obtain deswollen sample with weight of w_2. Then, cross-link density (γ) is calculated by the equation[43,44]

$$\gamma = \varphi^{5/3} \times G_f \quad (2)$$

DOI: 10.1021/acs.macromol.7b01068
Macromolecules 2017, 50, 5729−5738

where φ is the equilibrium volume fraction during swelling and G_f is the gel fraction of the sample. φ can be calculated by the equation

$$\varphi = \frac{w_0/\rho_2}{w_1/\rho_1 + w_0(1/\rho_2 - 1/\rho_1)} \quad (3)$$

where ρ_1 and ρ_2 are the densities of solvent (1.53 g cm^{-3}) and ESO thermosets (various for different samples), respectively. G_f is calculated by

$$G_f = \frac{w_2}{w_0} \times 100\% \quad (4)$$

2.9. Water Absorption Measurement. The water absorption of the NESO thermosets was measured by water immersing method. The sample sheet with dimension of 10 mm × 10 mm × 0.5 mm and weight of w_1 was immersed in distilled water at room temperature for 24 h and then were taken out of the water. The weight (w_2) was measured after wiping surface free water with filter paper. The water absorption was calculated by $(w_2 - w_1)/w_1 \times 100\%$. Three measurements were performed for each sample, and the averaged results were reported.

2.10. X-ray Diffraction (XRD). XRD diffraction patterns of NYL oligomers and the cured NESO thermosets were recorded on an X-ray diffractometer (Philips X'Pert X-ray diffractometer) with Cu Kα radiation at room temperature in the 2θ range of 5°−40° with a scan rate of 2°/min.

2.11. Differential Scanning Calorimetry (DSC). DSC thermograms were recorded on a NETZSCH instrument DSC-214 under a N_2 atmosphere. About 7 mg sample in an aluminum DSC pan was first melted at 200 °C for 3 min to remove thermal history and then cooled to −50 °C at a rate of 10 °C. After keeping for 3 min, they were finally reheated to 200 °C at the same rate. Both cooling and the second heating curves were recorded for analysis.

2.12. Thermogravimetric Analysis (TGA). Thermal stability was studied by a TA Instruments TGA Q500 from 50 to 650 °C at a heating rate of 10 °C/min under a N_2 atmosphere.

2.13. Dynamic Mechanical Analysis (DMA). The dynamic mechanical properties were measured on a TA Instruments DMA Q800 analyzer using a tensile mode from −60 to 190 °C at a heating rate of 3 °C/min and an oscillation frequency of 1 Hz. The samples with dimension of 35 mm (length) × 6 mm (width) × 0.5 mm (thickness) were used for the measurement.

2.14. Tensile Properties. Tensile properties were tested on a MTS E44 universal testing machine under a crosshead speed of 20 mm/min at room temperature (~25 °C). The standard dumbbell-shaped specimen with width and thickness of 4.0 and 0.5 mm was cut from the sample sheet. The length between the two pneumatic grips was 25 mm. At least five measurements were performed for each sample, and the averaged result was reported.

3. RESULTS AND DISCUSSION

3.1. Curing Behavior. NYL oligomer with different chain length was prepared by melt condensation of DD and SA with molar ratio of 1:2, 2:3, 3:4, and 4:5 at 210 °C under a N_2 atmosphere for 5 h, as shown in Scheme 1a. The obtained NYL oligomers are white and brittle solids. We characterized the chemical structure of the NYL oligomers via ^{1}H NMR (Supporting Information, Figures S1−S4). As evaporation of DD occurred during condensation reaction at 210 °C, some SA residue remained in the oligomer, as evidenced by the higher value of peak density ratio of b + b′ (proton of methylene linked to carbonyl of ester group and acid group) to a (proton of methylene linked to N atom) compared to the feed ratio. The content of the SA residue and the carboxyl content of the oligomers were calculated according to the related peak density ratio. The carboxyl content (Supporting Information, eqs S1−S3) is 4.15, 2.45, 1.74, and 1.42 mol/1000 g for NYL-1, NYL-2, NYL-3, and NYL-4, respectively. Considering the dicarboxyl-terminated structure of oligomers, the average molecular weights can be deduced as 482, 816, 1149, and 1408 g/mol for NYL-1, NYL-2, NYL-3, and NYL-4, respectively. The theoretical average degree of polymerization ($\bar{X}_n$) can be calculated through $2n + 1$ (n is the feed mole number of DD) by assuming the monomer conversion p was 1.0. The theoretical average molecular weight was calculated to be 540, 878, 1216, and 1554 g/mol for NYL-1, NYL-2, NYL-3, and NYL-4, respectively. It is obvious that the theoretical average molecular weights are higher than the corresponding measured values, possibly due to the incomplete conversion of monomers combined with the inevitable evaporation of DD during reaction. The carboxyl content was used to determine the feed ratio of NYL to ESO in fabrication of the all plant oil derived epoxy thermoset. For both nonisothermal and isothermal curing, the acid/epoxy equivalent ratio was fixed at 0.7.[26,44]

Scheme 1. Preparation of Dicarboxyl-Terminated Polyamide1010 Oligomers (a) and the Proposed Curing Reaction between Polyamide1010 Oligomers and Epoxidized Soybean Oil for Preparation of All Plant Oil Derived Epoxy Thermoset (b)

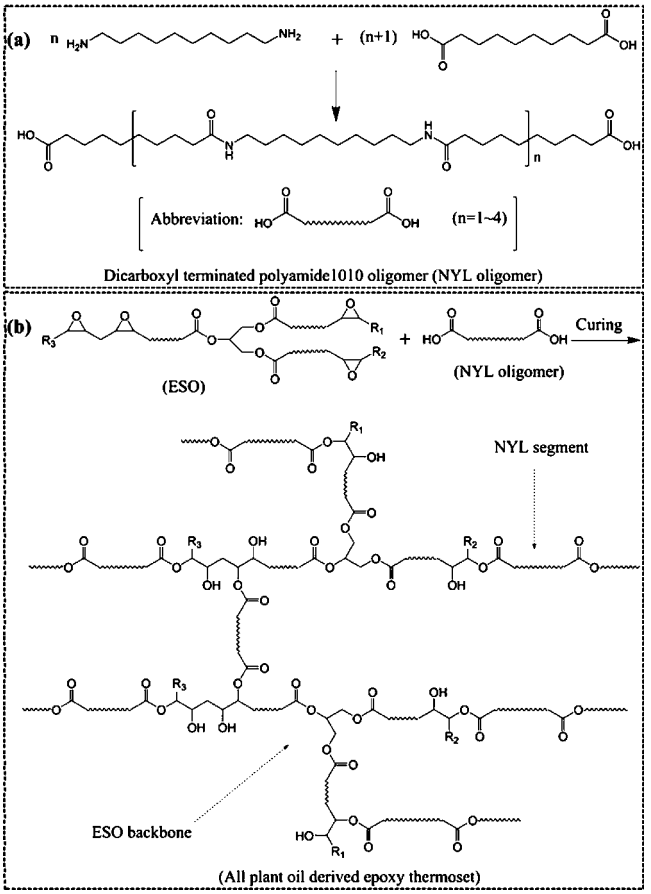

The rheological behaviors such as viscosity and modulus undergo immense change during curing process of thermosets.[45] Chemorheology, studying the rheological properties of reactive polymer system,[17] is used to investigate the curing of ESO with NYL oligomers. Scheme 1b shows the proposed curing reaction between ESO and NYL for preparation of all plant oil derived epoxy thermosets. We first studied the nonisothermal curing behavior of ESO with different chain-

DOI: 10.1021/acs.macromol.7b01068
Macromolecules 2017, 50, 5729−5738

lengthed NYL oligomers to show their effect on the curing behavior.

Figure 1 shows the development of complex viscosity and storage modulus as a function of temperature for the

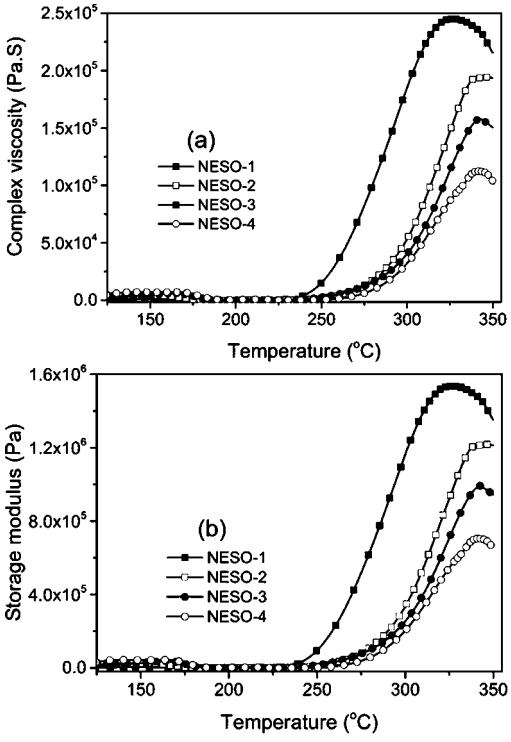

Figure 1. Complex viscosity (a) and storage modulus (b) as a function of temperature for nonisothermal curing of ESO and NYL oligomers with different chain length.

nonisothermal curing of ESO with NYL with different chain lengths. For brevity, we abbreviated the samples prepared from curing of ESO with NYL-1, NYL-2, NYL-3, and NYL-4 to NESO-1, NESO-2, NESO-3, and NESO-4, respectively. Both complex viscosity and storage modulus are higher than zero at low temperature due to the presence of NYL solid powders. A small drop in both complex viscosity and storage modulus plots occurs with the temperature increased to ~190 °C, corresponding to the melt of NYL powders. Complex viscosity and storage modulus remain unchanged with temperature increase to ~230 °C; thereafter, they begin to increase exponentially with further increase in the temperature, indicating occurrence of curing. The curing temperature increases with the chain length of NYL, as indicated by the shift of the curves to higher temperature range. The results indicate that the curing reactivity decreased with increase in the chain length of NYL, possibly due to higher probability of entanglement of the polymeric or oligomeric chains with increasing chain length, which would increase the steric hindrance of the curing reaction. Similar behaviors were observed for the curing of some other epoxy resins with dicarboxylic acids or diamines with different chain lengths.[25,46]

Both complex viscosity and storage modulus reach a maximum value with temperature continuously increases. Finally, a drop of all curves occurs, which may correspond to the disruption of the network structure due to thermal degradation at such high temperatures (higher than 325 °C). Interestingly, the maximum complex viscosity and storage modulus decrease with increasing NYL chain length, ascribing to the decreased cross-link density due to the increased chain length, which decreases the elastic response of the thermosets to exhibit lower storage modulus and complex viscosity.

We also studied the effect of chain length of NYL on the isothermal curing behavior of the reaction system. Figure 2

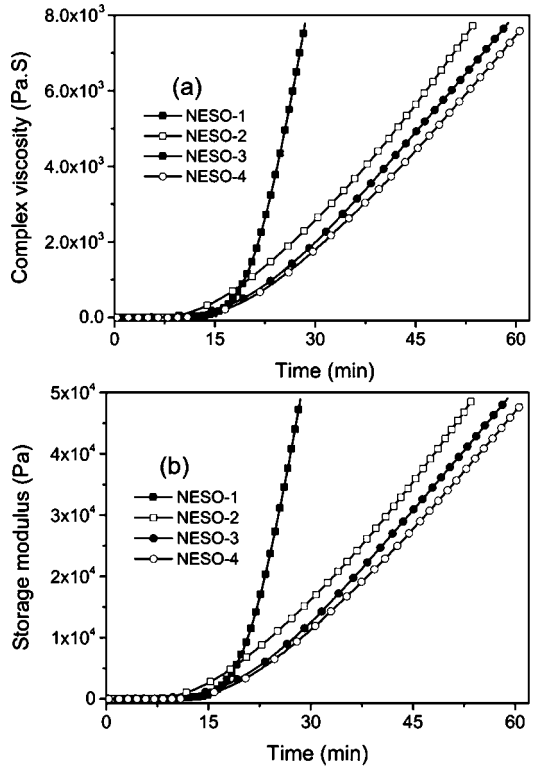

Figure 2. Complex viscosity (a) and storage modulus (b) as a function of time for isothermal curing of ESO and NYL with different chain lengths.

shows the development of complex viscosity and storage modulus as a function of time during isothermal curing at 210 °C. In the early stage within 10 min, both complex viscosity and storage modulus remain unchanged with low value close to zero, corresponding to the branching of the system.[45] Then, they grow exponentially with time proceeding due to the formation of network structures. The growth in the rheological parameters of NESO-1 is slower than the other three samples, possibly due to the presence of much SA residue in NYL-1. SA possesses much lower molecular mass compared to the oligomers, thus resulting in slower growth in molecular weight to exhibit relatively slow growth rate in the beginning. To study the effect of NYL chain length on the isothermal curing in detail, the gel point, the appearance of gel by the advancement of reactions during cure, was determined at the point when the steady shear viscosity reaches 10^3 Pa·s and the resins cease to flow readily.[47] The gel points for isothermal curing of ESO with NYL-1, NYL-2, NYL-3, and NYL-4 at 210 °C are 19.4, 20.1, 23.6, and 24.7 min, respectively, which also indicates that the curing reactivity decreases gradually with increasing NYL chain length.

3.2. Sample Preparation. Curing continues after gel point, as evidenced by the continuously developed complex viscosity and storage modulus with increasing time after gel point. It is hard to predict the terminal point of the curing system through

DOI: 10.1021/acs.macromol.7b01068
Macromolecules 2017, 50, 5729−5738

rheological measurement due to the infinite increase in the parameters. In order to obtain a criterion to direct sample preparation, we monitored the gel fraction with time during isothermal curing at 210 °C, as shown in Figure 3. Gel fraction

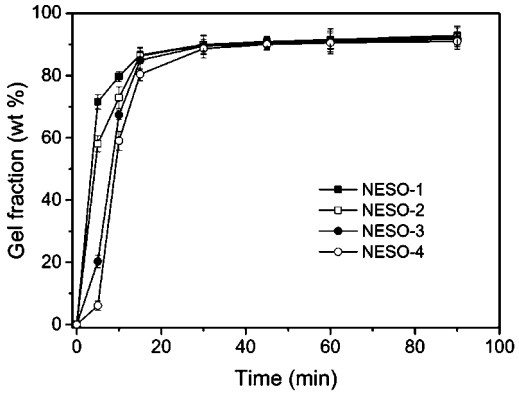

Figure 3. Gel fraction as a function of time for isothermal curing of ESO and NYL with different chain lengths at 210 °C.

increases significantly to ~88 wt % with the time increases to 30 min for all samples, indicating that curing occurred successfully. It is interesting that the sample with shorter chained NYL showed a higher gel fraction at 5 and 10 min, also indicating that the shorter the chain length, the higher the reactivity. Thereafter, the gel fraction increases very slightly with prolonged time. The gel fraction at 60 min is 89.9, 90.2, 91.1, and 89.5 wt % for NESO-1, NESO-2, NESO-3, and NESO-4, respectively. With curing time further increases to 90 min, the gel fraction changes very slightly. We collected the soluble parts of the final thermosets after gel fraction measurement by evaporation of the solvent, performed ^{1}H NMR for the soluble products of NESO-2 (Figure S6), and compared its ^{1}H NMR spectrum with those of ESO (Figure S5) and NYL-2 (Figure S2). Most of the characteristic signals belonging to ESO can be observed in the spectrum of the soluble part. Epoxy group of ESO disappeared in the soluble product due to the absence of $\delta(H^g)$ and the presence $\delta(H^l)$ and $\delta(H^k)$. In addition, some weak signals belonging to NYL $\delta(H^a)$ could also be observed. The results may indicate the formation of some soluble branched products by reaction of NYL and ESO during curing.

As introduced in the Experimental Section, we prepared the sample sheets of NYL cured ESO thermosets through a two-step curing method. In order to avoid phase separation between ESO and NYL, we precured ESO and NYL at 210 °C for ~10 min to yield a homogeneous melt. The precuring time, determined according to rheological measurement combined with gel fraction measurement, is a very important parameter for the sample sheet preparation. If the precuring time is shorter, the surface of the final cured thermosets feels very oily, possibly due to the insufficient curing reaction caused by phase separation of ESO and NYL. While if the precuring time is too long, uniform thermosets are also unavailable due to the formation of highly cross-linked structure during precuring. After precuring, the precursors were further cured at 210 °C under 10 MPa for ~50 min to yield the final thermosets.

We characterized the structure of NESO by FT-IR. Figure 4 shows the FT-IR spectra of ESO, NYL-2, and the typical NESO-2. It is obvious that the characteristic absorptions of oxirane at 843 and 960 cm^{-1} are absent in the spectrum of

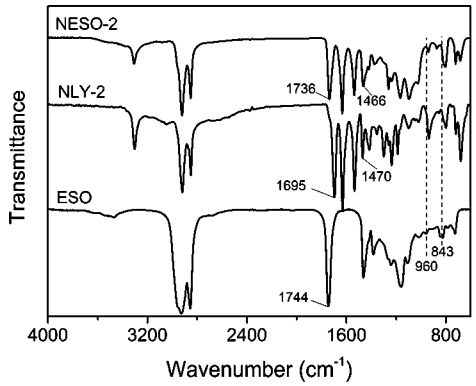

Figure 4. FT-IR spectra of ESO, NYL-2, and the typical NESO-2.

NESO-2, indicating curing of ESO took place sufficiently. The C−N absorption of NYL-2 (1470 cm^{-1}) is present in the spectrum of NESO-2, demonstrating that NYL was incorporated into NESO after curing. In addition, the position of carbonyl of NESO-2 (1736 cm^{-1}) is observed among that of ESO (1744 cm^{-1}) and NYL-2 (1695 cm^{-1}). We measured the cross-link density of the NESO thermosets via the solvent immersion method. With increase in chain length of NYL, the cross-link density decreases gradually, to be 0.038, 0.035, 0.034, and 0.027 mol cm^{-3} for NESO-1, NESO-2, NESO-3, and NESO-4, respectively.

Figure 5a−e shows the digital photos of the NYL oligomer cured ESO resins as well as the SA cured ESO thermoset (control sample). All the samples show slight yellow and transparent appearance. The color arises from the original color of ESO. It is obvious that the transparency reduces gradually with increasing NYL chain length, possibly due to the enhanced crystallization, which usually results in increased opaqueness of polymers.

In order to study the transparency of the samples quantitatively, we recorded the UV−vis spectra of the samples, as shown in Figure 5f. The sample shows good shielding effect toward ultraviolet as the transmittance of the samples in ultraviolet region is almost zero. With the increasing wavelength, the transmittance increases obviously, indicating lowered shielding effect toward visual light, namely, increased transparency. The transmittance decreases apparently with increasing NYL chain length at a given wavelength. For example, the values of the control is 63.2% at 700 nm, while those of NESO-1, NESO-2, NESO-3, and NESO-4 decrease gradually to 59.4, 49.6, 34.3, and 27.6%, respectively, attributing to the enhanced crystallization with increasing NYL chain length. In order to confirm this speculation, we studied the crystallization behavior of the samples by DSC and XRD in the next section.

3.3. Crystallization Behavior and Thermal Transition.

We first evaluated the crystallization behavior of ESO thermosets by X-ray diffraction. Figure 6 shows the XRD patterns of NESO thermosets and the control as well as NYL oligomers. All NYL oligomers are crystalline with obvious characteristic diffraction peaks at 2θ of 8.1°, 19.9°, and 24.0° (Figure 6a), corresponding to the (002), (100), and (010) planes, respectively.[48] An extra diffraction peak at 21.5° of NYL-1 should be ascribed to the presence of relatively high content of SA residues. The characteristic diffraction peaks of all planes of NYL are present in the diffraction patterns of all NESO thermosets although the peak intensity of (010) plane

DOI: 10.1021/acs.macromol.7b01068
Macromolecules 2017, 50, 5729−5738

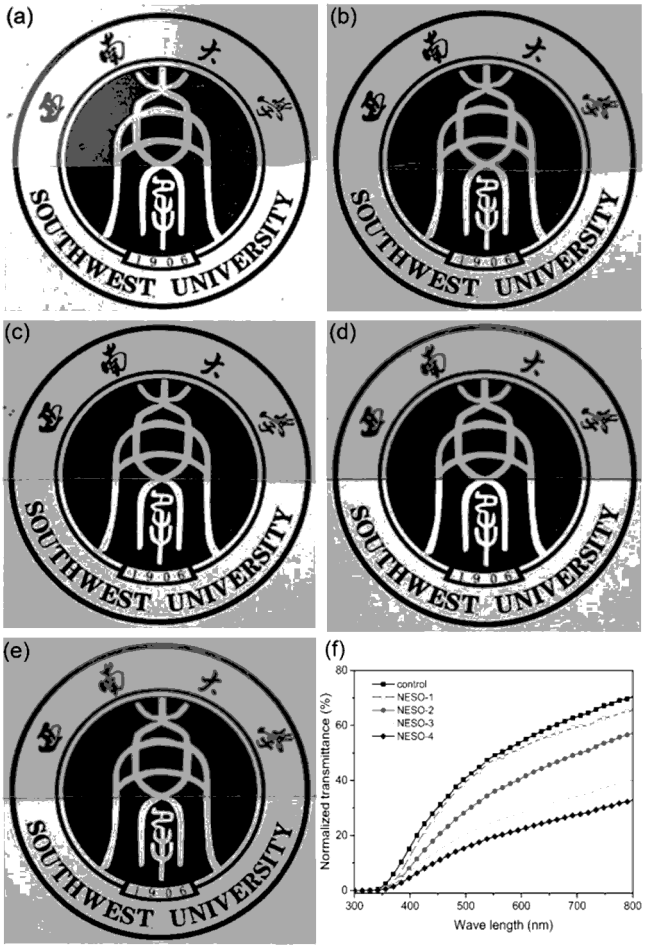

Figure 5. Digital photos of control (a), NESO-1 (b), NESO-2 (c), NESO-3 (d), and NESO-4 (e) as well as the UV−vis spectra of the control and the NESO thermosets.

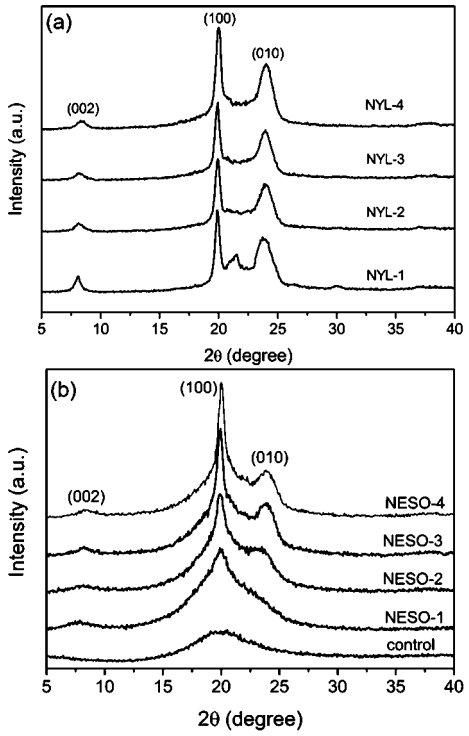

Figure 6. XRD patterns of NYL oligomers (a) and NESO thermosets (b) as well as the control prepared by curing ESO with SA.

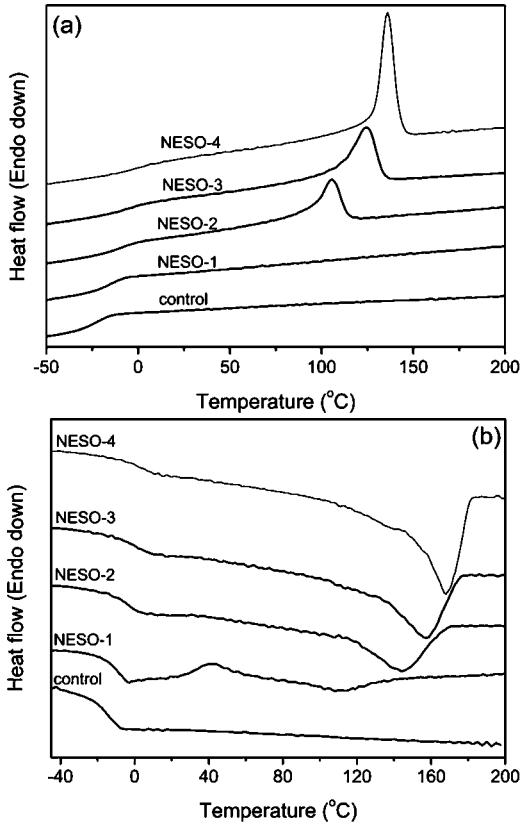

Figure 7. DSC cooling and the second heating scans of the control and NESO thermosets.

for NESO-1 is very weak, indicating that the crystallizability of NYL segments remain after incorporation into the NESO thermosets. The sharpness and intensity of the diffraction peaks of the thermosets reduce obviously compared to those of the NYL oligomers, which indicates that the crystallization of NYL segments depresses after incorporation into the thermosets due to the restricted chain mobility through chemical linkage with ESO. The intensity of the diffraction peaks increases gradually with increasing NYL chain length, indicative of enhanced crystallization, due to the less restriction in chain mobility of NYL with increasing its chain length. In contrast, the control sample prepared by curing of ESO with SA only shows an amorphous broad peak, indicating that the carbon chain of sebacic acid after incorporation into ESO thermoset is unable to crystallize.

We further studied the crystallization behavior and thermal transition of NESO thermosets via DSC. Figure 7 shows the DSC cooling and the second heating scans of NESO thermosets and the control. NESO-1 does not show a crystallization peak during the cooling process, while the other three NESO samples show an obvious crystallization peak and the crystallization enthalpy (ΔH_c) increases; meanwhile, the crystallization peak temperature (T_c) shifts to higher temperature range with increasing NYL chain length, indicating enhanced crystallization. The corresponding parameters are summarized in Table 1. NESO-1 is also crystalline, as evidenced by the presence a cold crystallization peak on the subsequent heating scan. All NESO samples exhibit an obvious melting peak. Both the melting temperature (T_m) and enthalpy of

DOI: 10.1021/acs.macromol.7b01068
Macromolecules 2017, 50, 5729−5738

Table 1. Parameters for Thermal Transition and Crystallization Behavior of NESO and the Control Obtained from DSC Curves

sample	T_g (°C)	T_c (°C)	ΔH_c (J/g)	T_m (°C)	ΔH_m (J/g)	X_c (%)
control	−14.2					
NESO-1	−10.2	43.8	4.9	108.3	5.1	5.0
NESO-2	−3.3	105.6	25.5	144.0	26.4	19.6
NESO-3	0.8	124.4	36.2	157.5	36.9	23.9
NESO-4	3.5	135.9	48.6	167.8	49.1	29.8

fusion (ΔH_m) increase with increasing NYL chain length due to the improved crystal perfection. The degree of crystallinity (X_c) of NYL segment in the thermoset was calculated by the equation

$$X_c = \frac{\Delta H_m}{f\Delta H_m^\circ} \times 100\% \quad (5)$$

where ΔH_m° is the melting enthalpy of 100% crystalline PA1010 (244.0 J g^{-1})[49] and f is the weight fraction of NYL segment in the thermoset. The value, as shown in Table 1, increases gradually with increasing chain length of NYL segment due to the enhanced crystallization. In contrast, the control shows only glass transition without crystallization and melting peaks in the scans, corresponding to its amorphous structure. All NESO thermosets show a single glass transition, indicating a homogeneous structure of the thermosets. The glass transition temperature (T_g) increases with increasing NYL chain length, which is explained by the increased weight content of NYL, which showed a high T_g with the value of 64.4 °C.[49] We also recorded the DSC cooling and the second heating scans of NYL oligomers (Figure S7) for comparison. Each NESO thermoset shows lower T_c, ΔH_c, T_m, and ΔH_m than the corresponding NYL oligomer (Table S1), ascribing to depressed crystallization of NYL segments after incorporation into the network thermoset through chemical bond linkage. It is interesting to find that NYL-1 shows multiple melting peaks due to the presence of SA residues. While NESO-1 shows a single melting peak, which is due to the absence of SA residue, due to transformation into thermoset, in which the carbon chain of SA moiety are unable to crystallize despite the crystalline nature of SA itself.

3.4. Mechanical Properties. We measured the static mechanical properties of the samples via tensile testing. Figure 8a shows the stress−strain curves of the as-prepared samples. The control sample shows a typical brittle and weak behavior with tensile strength (σ) and elongation at break (ε) of only 0.43 ± 0.09 MPa and 17 ± 2%, respectively. In contrast, the NESO thermosets show excellent mechanical properties with significantly enhanced tensile strength and elongation at break. The σ values increase significantly and continuously, while the ε values first increase drastically and then decrease apparently with increasing NYL chain length. The tensile strength increases by 16, 47, 46, and 59 times to 7.09 ± 0.44, 20.51 ± 0.87, 20.10 ± 1.27, and 25.82 ± 1.53 MPa for NESO-1, NESO-2, NESO-3, and NESO-4, respectively, compared to the control. The relatively higher σ value of NESO-2 than NESO-3 is due to the more extensive strain hardening arisen from the much higher elongation at break. The Young's modulus of the control is 2.6 ± 0.5 MPa, which significantly increases to 17.6 ± 2.5, 150.7 ± 2.4, 214.7 ± 21.1, and 378.1 ± 10.8 MPa for NESO-1, NESO-2, NESO-3, and NESO-4, respectively. The enhancement is 7, 58, 82, and 145 times compared to the control. The reinforced strength and modulus are reasonably attributed to the enhanced crystallinity of the samples with increasing NYL chain length. The ε values of NESO-1, NESO-2, NESO-3, and NESO-4 are 266 ± 15, 321 ±

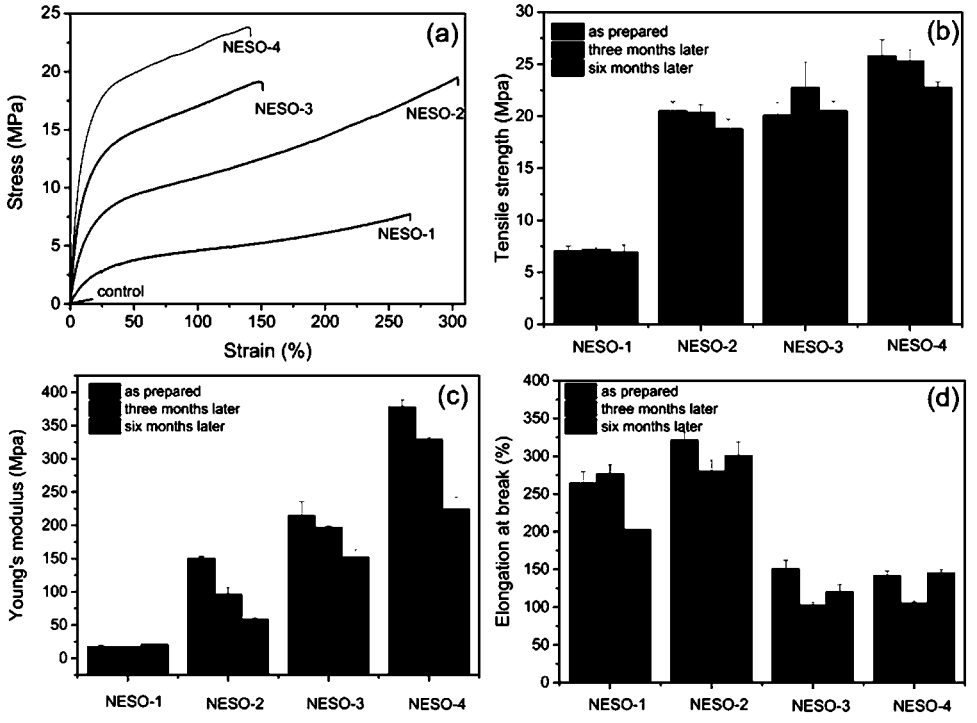

Figure 8. Stress−strain curves of NESO and the control (a), tensile strength (b), Young's modulus (c), and elongation at break (d) of NESO after storing for different times.

DOI: 10.1021/acs.macromol.7b01068
Macromolecules 2017, 50, 5729−5738

10, 151 ± 11, and 142 ± 6%, which are 16, 18, 9, and 8 times that of the control. The improved elongation at break of NESO samples compared to the control is attributed to the reduced cross-link density and enhanced network flexibility with increasing NYL chain length. The reduced elongation at break of NESO-3 and NESO-4 compared to NESO-2 may be explained by the increased degree of crystallinity. The results supported our idea of using long-chained crystalline curing agent to reinforce mechanical strength via enhancing crystallization and to improve ductility through reducing cross-link density.

In order to indicate the durability of NYL cured ESO thermosets, we measured the mechanical properties of the samples after storage at room temperature for different periods. Figure 8b–d summarizes the mechanical parameters of as-prepared NESO samples and the sample after storage for 3 and 6 months. Both the tensile strength and elongation at break change vary slightly although the Young's modulus reduced gradually with increasing storing time, indicating that the NYL cured ESO thermosets exhibit good durability and could find some durable applications. The reduced Young's modulus during storage may be attributed to the moisture absorption of the thermosets due to the presence of hydrophilic hydroxyl and amide groups, which make the thermosets somewhat moisture sensitive. We measured the water absorption of the NESO thermosets by immersing in distilled water until absorption equilibrium (24 h). The final water uptake values are 2.11 ± 0.05, 2.03 ± 0.07, 1.72 ± 0.10, and 1.19 ± 0.08 wt % for NESO-1, NESO-2, NESO-3, and NESO-4, respectively. The reduced water uptake should be attributed to the relatively reduced hydroxyl content and the enhanced degree of crystallinity, as discussed in the above text, with increasing NYL chain length.

Besides the static mechanical properties, we also studied the dynamic mechanical properties of the NYL cured ESO thermosets. Figure 9 shows the variation of storage modulus and tan δ with temperature for NESO thermosets and the control. The control exhibits only one slope in the storage modulus plots due to the amorphous structure, while the NESO thermosets show two slopes, corresponding to the glass transition and melting of the thermosets, respectively. The storage moduli of NESO thermosets are higher than the control in the full temperature range and increase gradually with increasing NYL chain length at given temperatures, indicating reinforced mechanical properties due to the enhanced crystallization. For example, the storage modulus of the control at 30 °C is only 0.9 MPa, while those of NESO-1, NESO-2, NESO-3, and NESO-4 are 22.4, 144.3, 215.6, and 435.5 MPa, which are about 25, 160, 240, and 484 times that of the control, respectively. Furthermore, we found that the heat resistance of the NESO thermosets improves with increasing NYL chain length, as the high storage modulus maintains to higher temperatures, which is attributed to the higher melting temperature of NYL crystals with increasing chain length. Corresponding to the storage modulus plots, one loss peak occurs for the control and two loss peaks appear for the NESO thermosets. The low peak temperature corresponds to the T_g of the samples. The value is −8.6 °C for the control, which deviates from the value obtained by DSC measurement, due to the different mechanisms of the two technologies. In agreement with the results obtained by DSC, NESO shows higher T_g than the control and the value increases with increasing NYL chain length. Interestingly, the control shows much higher damping peak than NESO thermosets. The damping peak height of the

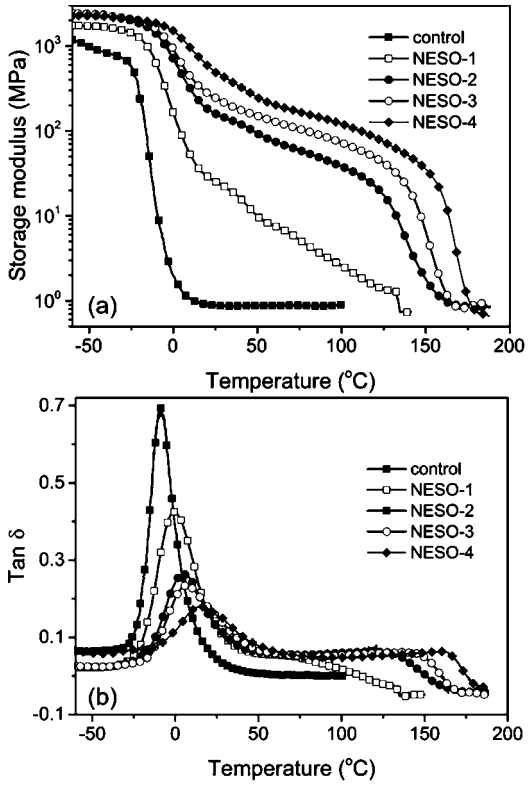

Figure 9. Storage modulus and tan δ as a function of temperature for NESO and the control.

NESO thermoset reduces gradually with increasing NYL chain length, again relating to the enhanced crystallization, which restricts the molecular movement thus lowers the damping in transition zone.[50]

3.5. Thermal Stability. The thermal stability of NESO thermosets was measured by TGA. Figure 10 shows the TGA and DTG curves of control and NESO thermosets under a N_2 atmosphere. The control shows a single weight loss stage with the maximum degradation temperature (T_{max}) of ∼429 °C. NESO samples show two weight loss stages with T_{max} of ∼429 and ∼489 °C, respectively. The weight loss at high temperature is caused by decomposition of NYL moiety since the loss value increases with increasing NYL chain length, and the weight loss at low temperature is attributed to the decomposition of ESO moiety. The onset decomposition temperature, T_5 (5% weight loss temperature), of control was 362 °C. The T_5 of NESO thermosets increases from 331 to 332, 373, and 381 °C with increasing NYL chain length due to the higher thermal stability of NYL moiety with higher chain length. Although the NYL chain length affects the thermal stability of the thermosets, it is worth noting that all NESO samples show good thermal stability since they all have onset temperature higher than 330 °C.

4. CONCLUSIONS

In summary, we report a facile way of fabricating all plant oil derived and high performance epoxy thermoset via catalyst-free curing of ESO with crystalline dicarboxyl-terminated polyamide1010 oligomer. The chain length of the oligomer not only influences the curing kinetics but also determines the final properties of the resultant epoxy thermoset. The curing temperature increases to higher temperature range during the

DOI: 10.1021/acs.macromol.7b01068
Macromolecules 2017, 50, 5729–5738

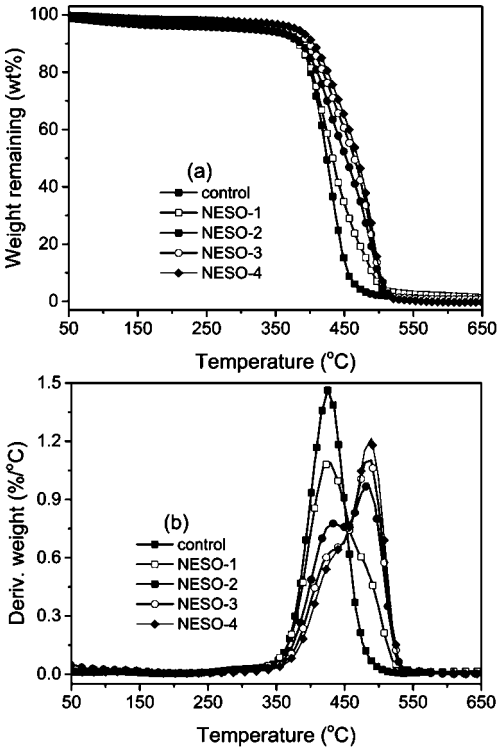

Figure 10. TGA (a) and DTG (b) curves of the control and NESO thermosets.

nonisothermal curing process, and the time required for finishing isothermal curing increases with increasing NYL chain length. The thermosets are crystalline, and the crystallization enhanced with increasing NYL chain length, which then impressively enhanced the tensile strength, Young's modulus, melting temperature, and heat resistance of the thermosets. Meanwhile, the thermosets showed excellent ductility due to the reduced cross-link density. The tensile strength and Young's modulus of crystalline NESO thermoset can be enhanced by up to 59 and 145 times, and the elongation at break can be improved by up to 18 times, compared to the amorphous ESO thermoset cured by short-chained sebacic acid. In addition, the thermosets show good durability and excellent thermal stability. The mechanical properties almost remained even after storage at room temperature for 6 months. The onset thermal decomposition temperature is as high as at least 330 °C. The study provided a novel way to fabricate high performance biobased epoxy thermoset, which is helpful for the future design and fabrication of some other sustainable epoxy thermosets.

■ ASSOCIATED CONTENT

Supporting Information

The Supporting Information is available free of charge on the ACS Publications website at DOI: 10.1021/acs.macromol.7b01068.

Procedures for NMR and DSC measurements, ^{1}H NMR analysis, DSC curves and data for polyamide1010 oligomers, and ^{1}H NMR of ESO and soluble parts of NESO (PDF)

■ AUTHOR INFORMATION

Corresponding Author

*E-mail: jbzeng@swu.edu.cn (J.B.Z.).

ORCID

Ming Wang: 0000-0003-2903-8064

Jian-Bing Zeng: 0000-0003-1822-446X

Notes

The authors declare no competing financial interest.

■ ACKNOWLEDGMENTS

This work was supported by National Science Foundation of China (51673158), the Basic and frontier research project of Chongqing (cstc2017jcyjAX0426), and Fundamental Research Funds for the Central Universities (XDJK2017A016 and XDJK2017C022).

■ REFERENCES

(1) Raquez, J. M.; Deleglise, M.; Lacrampe, M. F.; Krawczak, P. Thermosetting (bio)materials derived from renewable resources: A critical review. *Prog. Polym. Sci.* **2010**, *35*, 487−509.

(2) Montarnal, D.; Capelot, M.; Tournilhac, F.; Leibler, L. Silica-Like Malleable Materials from Permanent Organic Networks. *Science* **2011**, *334*, 965−968.

(3) Pham, H. Q.; Marks, M. J. Epoxy Resins. In *Ullmann's Encyclopedia of Industrial Chemistry*, Electronic Release; Elvers, B., Ed.; Wiley-VCH: Weinheim, 2012; pp 155−244.

(4) Wan, J.; Zhao, J.; Gan, B.; Li, C.; Molina-Aldareguia, J.; Zhao, Y.; Pan, Y.-T.; Wang, D.-Y. Ultrastiff Biobased Epoxy Resin with High T-g and Low Permittivity: From Synthesis to Properties. *ACS Sustainable Chem. Eng.* **2016**, *4*, 2869−2880.

(5) Auvergne, R.; Caillol, S.; David, G.; Boutevin, B.; Pascault, J.-P. Biobased Thermosetting Epoxy: Present and Future. *Chem. Rev.* **2014**, *114*, 1082−1115.

(6) Okada, H.; Tokunaga, T.; Liu, X.; Takayanagi, S.; Matsushima, A.; Shimohigashi, Y. Direct evidence revealing structural elements essential for the high binding ability of bisphenol A to human estrogen-related receptor-gamma. *Environ. Health Perspect.* **2007**, *116*, 32−38.

(7) vom Saal, F. S.; Hughes, C. An Extensive New Literature Concerning Low-Dose Effects of Bisphenol A Shows the Need for a New Risk Assessment. *Environ. Health Perspect.* **2005**, *113*, 926−933.

(8) Dodds, E. C.; Lawson, W. Synthetic strogenic Agents without the Phenanthrene Nucleus. *Nature* **1936**, *137*, 996.

(9) Chrysanthos, M.; Galy, J.; Pascault, J.-P. Preparation and properties of bio-based epoxy networks derived from isosorbide diglycidyl ether. *Polymer* **2011**, *52*, 3611−3620.

(10) Pan, X.; Sengupta, P.; Webster, D. C. High Biobased Content Epoxy-Anhydride Thermosets from Epoxidized Sucrose Esters of Fatty Acids. *Biomacromolecules* **2011**, *12*, 2416−2428.

(11) Ma, S.; Liu, X.; Jiang, Y.; Tang, Z.; Zhang, C.; Zhu, J. Bio-based epoxy resin from itaconic acid and its thermosets cured with anhydride and comonomers. *Green Chem.* **2013**, *15*, 245−254.

(12) Ma, S.; Webster, D. C. Naturally Occurring Acids as Cross-Linkers To Yield VOC-Free, High-Performance, Fully Bio-Based, Degradable Thermosets. *Macromolecules* **2015**, *48*, 7127−7137.

(13) Zhao, S.; Abu-Omar, M. M. Biobased Epoxy Nanocomposites Derived from Lignin-Based Monomers. *Biomacromolecules* **2015**, *16*, 2025−2031.

(14) Li, C.; Li, Y.; Cai, X.; Wang, H.; Bossmann, S. H.; Sung, J.; Sun, X. S. Competitive Nucleophilic Attack Chemistry Based on Undecenoic Acid: A New Chemical Route for Plant-Oil-Based Epoxies. *ACS Sustainable Chem. Eng.* **2016**, *4*, 5718−5729.

(15) Ma, S.; Webster, D. C.; Jabeen, F. Hard and Flexible, Degradable Thermosets from Renewable Bioresources with the Assistance of Water and Ethanol. *Macromolecules* **2016**, *49*, 3780−3788.

DOI: 10.1021/acs.macromol.7b01068
Macromolecules 2017, 50, 5729−5738

(16) Maiorana, A.; Reano, A. F.; Centore, R.; Grimaldi, M.; Balaguer, P.; Allais, F.; Gross, R. A. Structure property relationships of biobased n-alkyl bisferulate epoxy resins. *Green Chem.* **2016**, *18*, 4961−4973.
(17) Patel, A.; Maiorana, A.; Yue, L.; Gross, R. A.; Manas-Zloczower, I. Curing Kinetics of Biobased Epoxies for Tailored Applications. *Macromolecules* **2016**, *49*, 5315−5324.
(18) Li, P.; Ma, S.; Dai, J.; Liu, X.; Jiang, Y.; Wang, S.; Wei, J.; Chen, J.; Zhu, J. Itaconic Acid as a Green Alternative to Acrylic Acid for Producing a Soybean Oil-Based Thermoset: Synthesis and Properties. *ACS Sustainable Chem. Eng.* **2017**, *5*, 1228−1236.
(19) Wang, S.; Ma, S.; Xu, C.; Liu, Y.; Dai, J.; Wang, Z.; Liu, X.; Chen, J.; Shen, X.; Wei, J.; Zhu, J. Vanillin-Derived High-Performance Flame Retardant Epoxy Resins: Facile Synthesis and Properties. *Macromolecules* **2017**, *50*, 1892−1901.
(20) Zhao, S.; Abu-Omar, M. M. Renewable Thermoplastics Based on Lignin-Derived Polyphenols. *Macromolecules* **2017**, *50*, 3573−3581.
(21) Liu, Z. S.; Erhan, S. Z.; Xu, J. Y. Preparation, characterization and mechanical properties of epoxidized soybean oil/clay nanocomposites. *Polymer* **2005**, *46*, 10119−10127.
(22) Liu, Z.; Erhan, S. Z. Ring-Opening Polymerization of Epoxidized Soybean Oil. *J. Am. Oil Chem. Soc.* **2010**, *87*, 437−444.
(23) Li, A.; Li, K. Pressure-Sensitive Adhesives Based on Epoxidized Soybean Oil and Dicarboxylic Acids. *ACS Sustainable Chem. Eng.* **2014**, *2*, 2090−2096.
(24) Altuna, F. I.; Pettarin, V.; Williams, R. J. J. Self-healable polymer networks based on the cross-linking of epoxidised soybean oil by an aqueous citric acid solution. *Green Chem.* **2013**, *15*, 3360−3366.
(25) Ding, C.; Shuttleworth, P. S.; Makin, S.; Clark, J. H.; Matharu, A. S. New insights into the curing of epoxidized linseed oil with dicarboxylic acids. *Green Chem.* **2015**, *17*, 4000−4008.
(26) Zeng, R.-T.; Wu, Y.; Li, Y.-D.; Wang, M.; Zeng, J.-B. Curing behavior of epoxidized soybean oil with biobased dicarboxylic acids. *Polym. Test.* **2017**, *57*, 281−287.
(27) Teng, G. H.; Soucek, M. D. Epoxidized soybean oil-based ceramer coatings. *J. Am. Oil Chem. Soc.* **2000**, *77*, 381−387.
(28) Yang, D.; Peng, X.; Zhong, L.; Cao, X.; Chen, W.; Zhang, X.; Liu, S.; Sun, R. "Green" films from renewable resources: Properties of epoxidized soybean oil plasticized ethyl cellulose films. *Carbohydr. Polym.* **2014**, *103*, 198−206.
(29) Wang, X.-L.; Chen, L.; Wu, J.-N.; Fu, T.; Wang, Y.-Z. Flame-Retardant Pressure-Sensitive Adhesives Derived from Epoxidized Soybean Oil and Phosphorus-Containing Dicarboxylic Acids. *ACS Sustainable Chem. Eng.* **2017**, *5*, 3353−3361.
(30) Derksen, J. T. P.; Petrus Cuperus, F.; Kolster, P. Renewable resources in coatings technology: a review. *Prog. Org. Coat.* **1996**, *27*, 45−53.
(31) Lee, S.; Lee, K.; Kim, Y.-W.; Shin, J. Preparation and Characterization of a Renewable Pressure-Sensitive Adhesive System Derived from epsilon-Decalactone, L-Lactide, Epoxidized Soybean Oil, and Rosin Ester. *ACS Sustainable Chem. Eng.* **2015**, *3*, 2309−2320.
(32) Baroncini, E. A.; Yadav, S. K.; Palmese, G. R.; Stanzione, J. F. Recent advances in bio-based epoxy resins and bio-based epoxy curing agents. *J. Appl. Polym. Sci.* **2016**, *133*, 44103.
(33) Li, C.; Sung, J.; Sun, X. S. Network from Dihydrocoumarin via Solvent-Free Metal-Mediated Pathway: A Potential Structure for Substantial Toughness Improvement of Epoxidized Plant Oil Materials. *ACS Sustainable Chem. Eng.* **2016**, *4*, 1231−1239.
(34) Espana, J. M.; Sanchez-Nacher, L.; Boronat, T.; Fombuena, V.; Balart, R. Properties of Biobased Epoxy Resins from Epoxidized Soybean Oil (ESBO) Cured with Maleic Anhydride (MA). *J. Am. Oil Chem. Soc.* **2012**, *89*, 2067−2075.
(35) Ahn, B. K.; Kraft, S.; Wang, D.; Sun, X. S. Thermally Stable, Transparent, Pressure-Sensitive Adhesives from Epoxidized and Dihydroxyl Soybean Oil. *Biomacromolecules* **2011**, *12*, 1839−1843.
(36) Zhao, T.-H.; Wu, Y.; Li, Y.-D.; Wang, M.; Zeng, J.-B. High Performance and Thermal Processable Dicarboxylic Acid Cured Epoxidized Plant Oil Resins through Dynamic Vulcanization with Poly(lactic acid). *ACS Sustainable Chem. Eng.* **2017**, *5*, 1938−1947.
(37) Boquillon, N.; Fringant, C. Polymer networks derived from curing of epoxidised linseed oil: influence of different catalysts and anhydride hardeners. *Polymer* **2000**, *41*, 8603−8613.
(38) Miyagawa, H.; Misra, M.; Drzal, L. T.; Mohanty, A. K. Novel biobased nanocomposites from functionalized vegetable oil and organically-modified layered silicate clay. *Polymer* **2005**, *46*, 445−453.
(39) Altuna, F. I.; Esposito, L. H.; Ruseckaite, R. A.; Stefani, P. M. Thermal and Mechanical Properties of Anhydride-Cured Epoxy Resins with Different Contents of Biobased Epoxidized Soybean Oil. *J. Appl. Polym. Sci.* **2011**, *120*, 789−798.
(40) Mustata, F.; Tudorachi, N.; Rosu, D. Curing and thermal behavior of resin matrix for composites based on epoxidized soybean oil/diglycidyl ether of bisphenol A. *Composites, Part B* **2011**, *42*, 1803−1812.
(41) Naughton, F. C. Production, chemistry, and commercial applications of various chemicals from castor oil. *J. Am. Oil Chem. Soc.* **1974**, *51*, 65−71.
(42) Wang, Z.; Zhang, X.; Wang, R.; Kang, H.; Qiao, B.; Ma, J.; Zhang, L.; Wang, H. Synthesis and Characterization of Novel Soybean-Oil-Based Elastomers with Favorable Processability and Tunable Properties. *Macromolecules* **2012**, *45*, 9010−9019.
(43) Prasertsri, S.; Rattanasom, N. Fumed and precipitated silica reinforced natural rubber composites prepared from latex system: Mechanical and dynamic properties. *Polym. Test.* **2012**, *31*, 593−605.
(44) Jian, X.-Y.; He, Y.; Li, Y.-D.; Wang, M.; Zeng, J.-B. Curing of epoxidized soybean oil with crystalline oligomeric poly(butylene succinate) towards high performance and sustainable epoxy resins. *Chem. Eng. J.* **2017**, *326*, 875−885.
(45) Bidstrup, S. A.; Macosko, C. W. Chemorheology relations for epoxy-amine cross-linking. *J. Polym. Sci., Part B: Polym. Phys.* **1990**, *28*, 691−709.
(46) Chiu, Y.-C.; Huang, C.-C.; Tsai, H.-C.; Prasannan, A.; Toyoko, I. Effect of aromatic and aliphatic amines as curing agents in sulfone epoxy monomer curing process. *Polym. Bull.* **2013**, *70*, 1367−1382.
(47) Hou, T. H.; Huang, J. Y. Z.; Hinkley, J. A. Chemorheology of an epoxy-resin system under isothermal curing. *J. Appl. Polym. Sci.* **1990**, *41*, 819−834.
(48) Wang, B.; Wan, T.; Zeng, W.; Zhou, X.; Zhang, X. Crystallization and morphology of polyamide 1010/single-walled carbon nanotube nanocomposites under elevated pressure. *Polym. Int.* **2012**, *61*, 1462−1469.
(49) Yan, M.; Yang, H. Improvement of polyamide 1010 with silica nanospheres via in situ melt polycondensation. *Polym. Compos.* **2012**, *33*, 1770−1776.
(50) Nagarajan, V.; Zhang, K.; Misra, M.; Mohanty, A. K. Overcoming the Fundamental Challenges in Improving the Impact Strength and Crystallinity of PLA Biocomposites: Influence of Nucleating Agent and Mold Temperature. *ACS Appl. Mater. Interfaces* **2015**, *7*, 11203−11214.

DOI: 10.1021/acs.macromol.7b01068
Macromolecules 2017, 50, 5729−5738